3-11-2021

Computed Tomography-Derived 3D Modeling to Guide Sizing and Planning of Transcatheter Mitral Valve Interventions

Joris F. Ooms

Dee Dee Wang

Ronak Rajani

Simon Redwood

Stephen H. Little

See next page for additional authors

Authors

Joris F. Ooms, Dee Dee Wang, Ronak Rajani, Simon Redwood, Stephen H. Little, Michael L. Chuang, Jeffrey J. Popma, Gry Dahle, Michael Pfeiffer, Brinder Kanda, Magali Minet, Alexander Hirsch, Ricardo P. Budde, Peter P. De Jaegere, Bernard Prendergast, William O'Neill, and Nicolas M. Van Mieghem

JACC: CARDIOVASCULAR IMAGING VOL. ■, NO. ■, 2021

PUBLISHED BY ELSEVIER

iREVIEW

STATE-OF-THE-ART PAPER

Computed Tomography–Derived 3D Modeling to Guide Sizing and Planning of Transcatheter Mitral Valve Interventions

Joris F. Ooms, MD,[a] Dee Dee Wang, MD,[b] Ronak Rajani, MD,[c] Simon Redwood, MD,[d] Stephen H. Little, MD,[e] Michael L. Chuang, MD,[f] Jeffrey J. Popma, MD, PHD,[f] Gry Dahle, MD,[g] Michael Pfeiffer, MD,[h] Brinder Kanda, MD,[i] Magali Minet, MSC,[j] Alexander Hirsch, MD, PHD,[a,k] Ricardo P. Budde, MD, PHD,[k] Peter P. De Jaegere, MD, PHD,[a] Bernard Prendergast, MD,[c] William O'Neill, MD,[b] Nicolas M. Van Mieghem, MD, PHD[a]

ABSTRACT

A plethora of catheter-based strategies have been developed to treat mitral valve disease. Evolving 3-dimensional (3D) multidetector computed tomography (MDCT) technology can accurately reconstruct the mitral valve by means of 3-dimensional computational modeling (3DCM) to allow virtual implantation of catheter-based devices. 3D printing complements computational modeling and offers implanting physician teams the opportunity to evaluate devices in life-size replicas of patient-specific cardiac anatomy. MDCT-derived 3D computational and 3D-printed modeling provides unprecedented insights to facilitate hands-on procedural planning, device training, and retrospective procedural evaluation. This overview summarizes current concepts and provides insight into the application of MDCT-derived 3DCM and 3D printing for the planning of transcatheter mitral valve replacement and closure of paravalvular leaks. Additionally, future directions in the development of 3DCM will be discussed. (J Am Coll Cardiol Img 2021;■:■–■) © 2021 by the American College of Cardiology Foundation.

Pre-procedural planning with 3-dimensional (3D) multidetector computed tomography (MDCT) has proven to be a prerequisite planning tool for successful transcatheter aortic valve replacement (TAVR) in elderly patients with degenerative tricuspid aortic valve stenosis (AS) who are at elevated operative risk (1).

A plethora of catheter-based strategies aim to tackle mitral valve defects. Whereas the aortic root arguably represents a relatively straightforward tubular structure, the mitral valve features a more complex confluence of surrounding structures and introduces patient-specific particularities. This requires individualized advanced planning. Traditionally,

From the [a]Department of Interventional Cardiology, Thoraxcenter, Erasmus University Medical Center, Rotterdam, the Netherlands; [b]Center for Structural Heart Disease, Division of Cardiology, Henry Ford Health System, Detroit, Michigan, USA; [c]Department of Cardiology, Guy's and St. Thomas' NHS Foundation Trust, London, United Kingdom; [d]Cardiovascular Division, King's College London British Heart Foundation Centre of Excellence, The Rayne Institute, St. Thomas' Hospital Campus, London, United Kingdom; [e]Department of Cardiology, Houston Methodist Hospital, Houston, Texas, USA; [f]Cardiovascular Division, Department of Internal Medicine, Beth Israel Deaconess Medical Center, Boston, Massachusetts, USA; [g]Department of Cardiothoracic Surgery, Oslo University Hospital, Oslo, Norway; [h]Division of Cardiology, Penn State Heart and Vascular Institute, Hershey, Pennsylvania, USA; [i]Stroobants Cardiovascular Center, Lynchburg, Virginia, USA; [j]Materialise NV, Leuven, Belgium; and the [k]Department of Radiology and Nuclear Medicine, Erasmus University Medical Center, Rotterdam, the Netherlands.

The authors attest they are in compliance with human studies committees and animal welfare regulations of the authors' institutions and Food and Drug Administration guidelines, including patient consent where appropriate. For more information, visit the Author Center.

Manuscript received October 2, 2020; revised manuscript received December 16, 2020, accepted December 23, 2020.

ISSN 1936-878X/$36.00 https://doi.org/10.1016/j.jcmg.2020.12.034

ABBREVIATIONS AND ACRONYMS

3D = 3-dimensional

3DCM = 3-dimensional computational modeling

3Dp = 3-dimensional printing

LA = left atrium/atrial

LV = left ventricle/ventricular

LVOT = left ventricular outflow tract

LVOTO = left ventricular outflow tract obstruction

MAC = mitral annular calcification

MDCT = multidetector computed tomography

PVL = paravalvular leakage

THV = transcatheter heart valve

TMVR = transcatheter mitral valve replacement

echocardiography has been the mainstay of imaging. However, there are limitations to using single-modality imaging for transcatheter pre-procedural evaluation. Two-dimensional echocardiography is often unable to visualize the trajectory for intracardiac devices in relation to surrounding anatomic structures. 3D transesophageal echocardiography (TEE) has limited spatial resolution and may be hampered by dropout artifacts that may mimic perforations or leaks (2). It is this spatial resolution that is essential in complex catheter-based mitral interventions, as it enables adequate device sizing and detailed assessment of the valve and its surroundings.

Improvements in MDCT spatial resolution, acquisition speed, and reconstruction algorithms enable the derivation of accurate virtual 3D reconstructions of cardiac structures to virtually test catheter-based procedures. Compared with echocardiography and cardiovascular magnetic resonance imaging (CMR), MDCT has superior spatial resolution and allows for isotopical imaging. 3-dimensional printing (3Dp), based upon MDCT-derived 3D computational models, complements virtual modeling and offers the opportunity to implant devices in life-sized casts of the cardiac anatomy (3). The 3D-printed modeling facilitates hands-on procedural planning, device training, and retrospective procedural evaluation. Ultimately, physicians may better understand a patient's unique anatomy and can bench test future catheter-based interventions (4–6). A clear distinction has to be made between 3D computational models and *simulation*, the latter using tissue/device properties and their respective interactions to predict structural/functional outcome. Furthermore, by adding computational fluid dynamics to these models, blood flow is simulated (7).

Herein, we provide a comprehensive overview of MDCT-derived 3D modeling in transcatheter mitral valve procedures including computational (virtual) modeling and printing. We place this technology in the perspective of transcatheter mitral valve replacement (TMVR) and mitral paravalvular leakage (PVL) closure

BASIC PRINCIPLES OF MDCT-DERIVED 3D COMPUTATIONAL MODELING

The cornerstone of MDCT-derived 3D computational modeling (3DCM) and 3Dp is based upon the following individual guidelines for MDCT-acquisition, segmentation, and understanding of the proposed cardiac intervention using available cardiac imaging applications (4,8).

MDCT ACQUISITION. A detailed overview of MDCT image acquisition is beyond the scope of this paper, but in general, MDCT 3D modeling requires contrast-enhanced, electrocardiography-gated MDCT acquisition without too stringent electrocardiographic dose modulation. Iodinated contrast is injected intravenously at a rate of ≤4 ml/s. However, this may vary, as protocols between scanners, hospitals, and patients differ. The use of a saline/contrast flush should be determined based on indication. Image reconstruction should be performed for the entire cardiac cycle at 5% to 10% increments of the R-R interval resulting in 10 to 20 datasets per cardiac cycle. The reconstructed slice thickness should be <1 mm. Depending on the intracardiac region of interest and the procedure to be performed, specific phases in the cardiac cycle are selected for segmentation. The mid to late diastolic phase is required for maximal mitral annulus dimensions. Conversely, annular dimensions in the mid to late systolic phase are required for minimal mitral annular dimensions (8).

IMAGE SEGMENTATION. Image segmentation is a process in which an anatomic label is assigned to a set of pixels that share similar characteristics. Geometric analysis and sizing become possible as different anatomic structures emerge in the digital image. MDCT is the only modality able to isotopically image the heart, meaning that volume pixels (voxels) are identical in size in the x, y, and z planes. Manual segmentation of cardiac chambers, valves, and great vessels is time-consuming and has high interobserver variability. Specialized software packages offer (semi) automated segmentation processes (9,10) (**Figure 1**). In semiautomated segmentation, users label the cardiac structures and indicate thresholds for the gray value range in which those structures are optimally visualized. With this input, segmented 3D models of the heart chambers and great vessels are automatically obtained from MDCT images using either volume rendering (VoR) or computational modeling (CM) (**Figure 2**). In VoR, a grid of voxels is visualized using transparency and coloring. In CM, voxels are used to derive a mesh structure of a multitude of triangles (the amount depends on the level of convexity and detail requested). Although a VoR model allows rapid visualization of the grayscale in 3D, it has limited capabilities for downstream operations such as automated quantification. CM enables automated analysis of anatomic structures, provides enhanced spatial insight, and can be converted to a 3D-printed model. A

FIGURE 1 Heart Segmentation

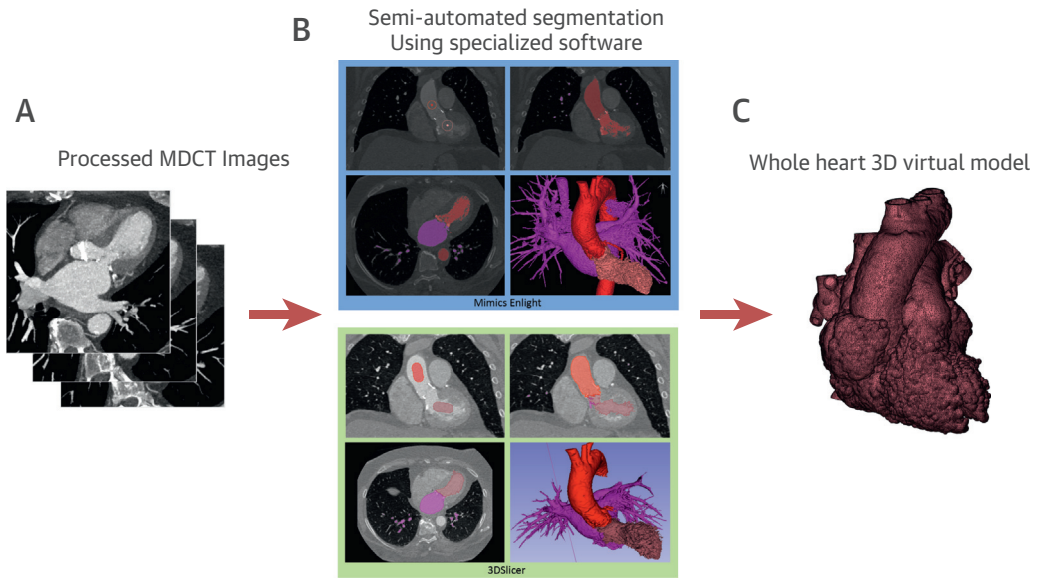

(A) Processed multidetector computed tomography (MDCT) images are loaded into specialized segmenting software. **(B)** Using dedicated software packages, essential cardiac structures such as the aorta **(red)** and left ventricle **(pink)** are marked after which the software semi-automatically identifies the MDCT-rendered volumes of the aorta, left ventricle, left atrium, and pulmonary vessels **(purple)**. From these data, segmented 3-dimensional (3D) computational models of the heart chambers and great vessels are automatically obtained. **(C)** The whole heart MDCT-derived 3D computational model can be printed or virtually assessed.

3D computational model can be converted to files with different extensions, serving different purposes. For example, the model might be saved as a stereolithographic file (.STL), facilitating 3Dp, or as an object file (.OBJ), enabling assessment in virtual reality. Most models in this paper are created using the CM method; alternative techniques are highlighted where applicable. Once cardiac structures are virtually modeled, a broad spectrum of clinical applications becomes available, including assessment of ventricular and atrial dimensions, characterizing heart defects, procedural planning, and the design and geometric validation of medical devices (10-13).

Various (semi)automated segmentation packages are available including but not limited to: Mimics Innovation Suite, 3D Slicer, Vitrea, TeraRecon, 3Mensio, Solidworks, and Vascular Modeling Toolkit (4). In this paper, the Mimics software package (Materialise NV, Leuven Belgium) was used unless stated otherwise.

GENERAL CONCEPTS IN 3D COMPUTATIONAL MODELING. Sizing an asymmetrical 3D orifice. As existing devices in structural heart disease are generally symmetrical and available in specific sizes, the key to pre-operative assessment is to match asymmetrical patient anatomy with symmetrical device shape. Sizing an asymmetrical 3D orifice can be challenging, and 2 methods are generally used.

The conventional method uses MDCT images (axial thin sections) to obtain a plane at the level of basal insertion of the mitral leaflets into the mitral annular ring creating a hinge-point during the mid to late diastolic phase of the ventricular cycle. Subsequently, using the double oblique view, the mitral annular dimensions are captured. This completely manual technique, which is de facto planimetry, relies heavily on operator experience to provide the accurate annular size and landing zone for a virtual transcatheter heart valve (THV) (10) (**Figures 2A and 2B**). This technique does not accurately reflect the 3D structure of the saddle-shaped mitral annulus. Its height, in particular, is challenging to incorporate.

In an alternative VoR-based method, the analyst tracks the mitral annulus using reference points in multiple planes around a user-defined center point (centrally located in the mitral orifice), which creates a 3D reconstruction of the mitral annulus (**Figures 2C and 2D**). In a method based on 3DCM, mesh models of the left atrium (LA), left ventricle (LV), and calcium (if present) are used to position mitral annular reference

FIGURE 2 Methods to Derive the Virtual Annulus Using MDCT

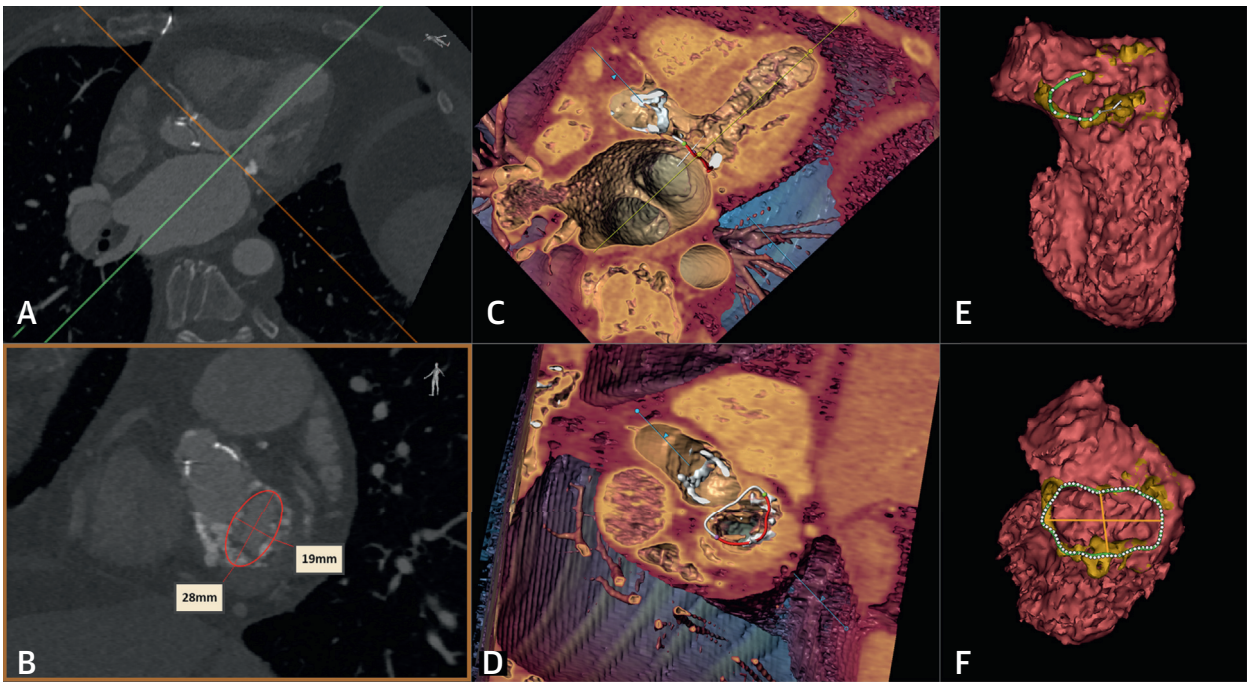

(A) Conventional sizing method: Cross-sectional view of the left heart including the large left atrium, left ventricle, and aortic valve prosthesis. The **orange line** represents the double oblique view visualized in **B**. **(B)** Axial thin section of the mitral annulus demonstrating severe mitral annular calcification. The **red ellipse** is manually fitted onto the annulus, allowing derivation of the maximal and minimal annular diameters. **(C)** Volume rendering method: a 3D annulus was created around a user-defined center point **(yellow dot). (D)** Atrial view, annular dimensions were: area derived Ø 26 mm, max. Ø 31 mm, min. Ø 20 mm. **(C and D)** Images were obtained with the 3Mensio software package. **(E)** 3D computational modeling method: a MDCT-derived 3D computational model of the left ventricle **(pink)** and mitral annular calcification **(yellow)** allows semiautomated mitral annulus tracing **(white reference points and green line)**. **(F)** Using reference points, a 3D virtual mitral annulus is computed and used to compute the best-fit plane **(orange lines)** and associated annular dimensions (area derived Ø 23 mm, max. Ø 30 mm, min. Ø 16 mm). **(E and F)** Images were obtained with the Mimics software package. All images originate from the same MDCT scan. Abbreviations as in Figure 1.

points (Figures 2E and 2F). From these references, dedicated software constructs a smooth 3D virtual annulus derived from a series of Fourier approximations for each of the spatial coordinates (x, y, z) (semiautomated). The contour of the annulus is then projected onto its best-fit plane, which is calculated using the least squares method (14) (Figure 2D). This projected annulus is used to derive the annular area and diameters. Consequently, the best-fit plane serves as the landing zone for the virtual THV implant. Compared with the conventional method in general, both the VoR and the 3D computational method allow for a 3D reconstruction of the mitral annulus. 3DCM further provides a full mesh model of the surrounding structures allowing detailed assessment of asymmetrical structures in a sole model. Furthermore, it enables semiautomated measurement of asymmetrical structures, volumes, and orifices reducing variability and potentially lessening processing time.

Virtual device implantation. MDCT-derived 3DCM allows fitting of a geometric shape or a digitalized 3D virtual device. An empirical starting point for device and size selection is the area-derived diameter of the reconstructed annulus or orifice. The selected device is automatically centered around the geometric midpoint of the best-fit plane. Given the asymmetrical shape of anatomic structures, it is essential to visually assess fitting of the device in multiple angles. Spatial interaction with surrounding structures can also be tested, thereby identifying possible malapposition or obstruction (9) (Figure 3). This concept of an adequate visual fit is essential in MDCT-derived 3DCM, but lacks any appreciation of tissue and device characteristics to interpret device-host interactions. Specialized models that incorporate tissue and device properties in virtual models are under development and have reasonable accuracy in TAVR simulation of implants and prediction of residual

FIGURE 3 **MDCT-Derived 3D Computational Model of the Left Heart With Severely Calcified Mitral Annulus**

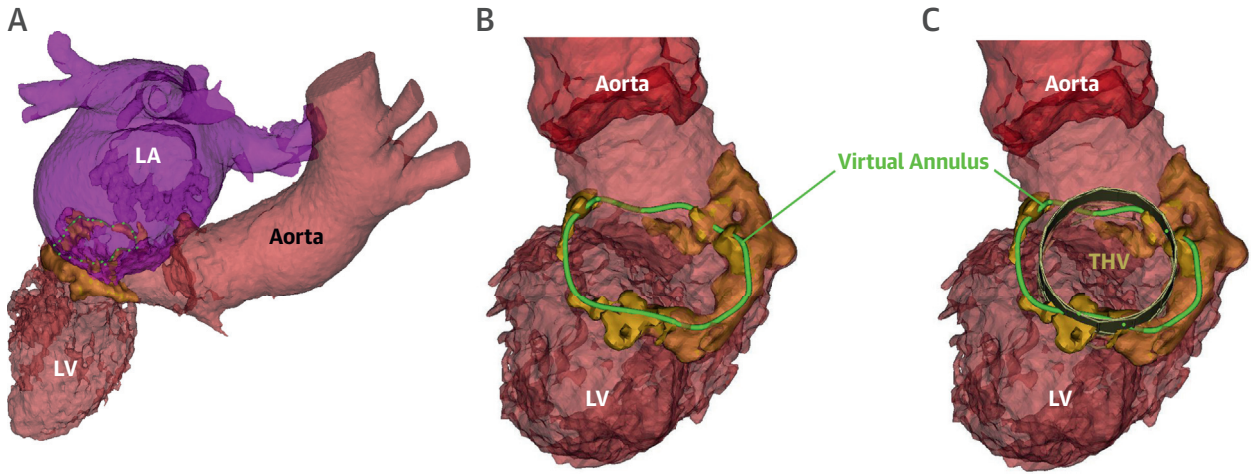

(A) MDCT-derived 3D computational modeled reconstructions of the left atrium (LA) and pulmonary veins **(purple)**, mitral annular calcification (MAC) **(yellow)**, left ventricle (LV), and aorta **(red)**. The mitral annulus is traced with **green dots**. MAC is used as a reference point for virtual annular construction **(green line)**. **(B)** Surgical view of the same calcified mitral annulus. **(C)** Virtual implantation of a cylinder representing a 23-mm Sapien3 transcatheter heart valve (THV) (Edwards Lifesciences, Irvine, California). Abbreviations as in Figure 1.

paravalvular leaks, conduction disorders, and calcium displacement (7,15).

3D PRINTING

MDCT-derived 3D computational models incorporate spatial relationships on a 2-dimensional screen and might impair complete understanding of the detailed 3D reality. Consequently, a full understanding of the model requires meticulous and time-consuming assessment from multiple angles. However, transformation of these computational (virtual) models into physical form by means of 3Dp can resolve these limitations. The availability of a patient-specific physical model can facilitate medical teaching, exploration of valve function, and pre-procedural planning (11). In congenital heart disease, 3Dp has been shown to be helpful in pre-procedural planning of surgical correction (16). Subsequently, this technique has been gradually adopted to help plan different catheter-based interventions for structural heart disease (4). In the mitral space, 3Dp models have been instrumental in the identification of defects, device sizing, and procedure execution (**Figure 4**) (11,17)

A recent systematic review on 3Dp in adult heart valve disease identified MDCT as the first choice modality for 3Dp (62%), followed by ultrasound (28%), computer aided design with separate manual creation of model parts (7%), and CMR (3%) (4). MDCT offers excellent spatial resolution, allowing clear depiction of pathological calcium and does not generally require image quality adjustment before anatomic segmentation (17). The TEE-derived 3Dp is limited by suboptimal detection of the subvalvular apparatus, left ventricular geometry, tissue differentiation, or calcium deposits. Additionally, because spatial resolution of ultrasound is best along the longitudinal plane, views from different angles need to be fused to capture 2 perpendicularly aligned structures and master resolution issues. Resolution is also limited by the probe-specific properties of the piezoelectric crystal. Ultimately, TEE does not allow for isotropic imaging and is therefore less suitable for 3Dp. CMR avoids radiation exposure and has excellent tissue characterization abilities, but is hampered by inferior spatial resolution that may impair detection of small intracardiac defects. However, it has been successfully applied to 3D-printed modeling in congenital heart disease (8).

3D-printed models in cardiovascular disease are typically composed of a variety of rigid and/or flexible materials (4,18,19). Rigid material, such as polybutylene terephthalate, acrylonitrile-butadiene styrene, and polyamide, are suited for mimicking prostheses and calcium. They can also be used if the goal of the print is to acquire complementary anatomic insight (educational purposes), regardless

FIGURE 4 Pre-Procedural Assessment Using 3D-Printed Models of the Mitral Valve

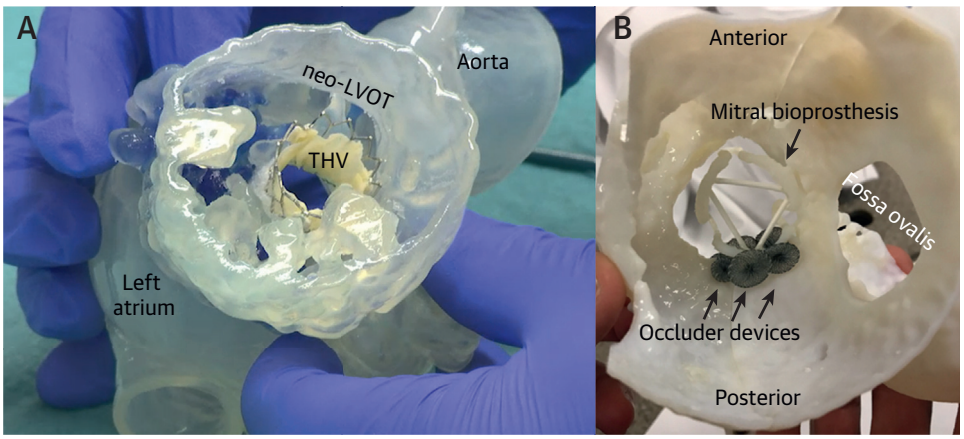

(A) MDCT-derived, 3D-printed model of the left heart with a 26-mm Sapien3 prosthesis implanted in the mitral annulus allowing for detailed evaluation of the expected neo-left ventricular outflow tract from a left ventricular viewpoint. **(B)** Surgeon's view of the left atrium of a 3D-printed model in which occluder devices are positioned along the frame of a bioprosthetic mitral valve. THV = transcatheter heart valve; other abbreviations as in Figure 1.

of any appreciation of tissue characteristics. Flexible materials, including, but not limited to, thermoplastic elastomers (i.e., Tango Plus, Agilus, HeartprintFlex) and printable silicones, are increasingly developed to mimic human tissue and are more suitable for fitting actual devices. Other materials, such as resins, can be used to yield either solid or flexible models depending on the printing technique used. By combining materials of different rigidity in 1 3D-printed model, valve calcification or the presence of a prosthetic valve can be replicated.

In practice, both healthy and diseased native valve tissue is highly heterogeneous with variable physical properties (20). Currently available 3Dp material does only slightly approach the properties of arterial tissue, and is still far away from reliably representing the human heart (17). The mechanical properties of the ideal printed model would resemble tissue-specific characteristics under different circumstances. In reality, however, a trade-off between practicality and cost determines the final 3D print. As such, 3Dp of the heart is still in its infancy and under further development.

CLINICAL APPLICATIONS OF 3D COMPUTATIONAL MODELING: TRANSCATHETER MITRAL VALVE REPLACEMENT

Mitral regurgitation and mitral stenosis are the second and third most frequent clinically relevant valve diseases (21). The advent of catheter-based techniques for mitral repair and replacement presents new treatments for a significant number of patients who would otherwise be denied conventional surgery (21). TMVR is beset by complex anatomic challenges, including its central cardiac location; elliptical, saddle-shaped annulus; and associated chordal apparatus. Additionally, it introduces the risk of left ventricular outflow tract (LVOT) obstruction (22,23) and valvular foreshortening in the LA. TMVR can be performed in previously surgically implanted annular rings, bioprostheses, and the native annulus (24-26).

A failing bioprosthesis, mitral ring, or excessive mitral annular calcification may provide anchoring opportunities for THV designs that were originally developed for aortic valve implantation (24,27). In the native noncalcified mitral annulus, the implanted valve uses other anchor opportunities and typically dominates its direct surroundings, which has consequences for the risks of PVL and left ventricular outflow tract obstruction (LVOTO). To address this, multiple dedicated designs for TMVR are under development or have entered clinical trials (25,28). MDCT-derived 3DCM may prove particularly helpful for TMVR, as various TMVR sizes and designs can be evaluated in virtual implants, generating information to enhance procedural efficacy and patient safety.

VIRTUAL ANNULUS CREATION AND VALVE SIZING. A surgical prosthesis is traceable on MDCT planimetry. Additionally, implanted prosthesis type and size can be deducted from these images, leading to a

relatively straightforward THV sizing and provision of a ready-made best-fit plane (29). However, blooming artifacts may affect measurements (30). Sizing the native mitral annulus (with/without annular calcium) proves more challenging as its borders are asymmetrical and less pronounced. In such cases, planimetry may omit important information. Additionally, the native annulus varies in size during the cardiac cycle, which warrants careful selection of cardiac phase when creating and measuring the virtual annulus. Its complex shape and close relation with the ventricle ideally require virtual 3D reconstruction as described in the section "General concepts in 3D computational modeling."

In the native mitral annulus, the trigone-to-trigone connection represents an additional landmark in this process (31). If necessary, subtle adjustments in the virtual mitral annulus shape can be made. The original annular anatomy may be severely distorted by mitral annular calcification (MAC), allowing limited use of common structural landmarks (9). However, calcification can be used as a landmark for annular sizing. In MDCT-derived 3DCM, calcium is segmented as a separate structure and integrated in the structural model, thereby facilitating virtual reconstruction of the mitral annulus (**Figures 2E, 2F, and 3**). Still, caution must be taken with annulus reconstruction based on MAC, as calcium may cause blooming artifacts and potentially affect adequate prosthesis sizing (32).

The virtually reconstructed mitral annulus facilitates automated calculation of the reference plane (best-fit plane, "General concepts in 3D computational modeling" section) on which a virtual prosthetic valve can be projected. Selecting multiple valve sizes/types, and shifting their position within the reconstructed annulus, helps to obtain an adequate visual fit (**Figure 3C**). However, as this is a virtual model without incorporation of tissue and device characteristics, in vivo malapposition still poses an important risk, especially in MAC (33).

NEO-LVOT. TMVR may cause LVOT deformation as a result of strut protrusion and anterior mitral leaflet (AML) displacement (34). This leads to the formation of a new elongation of the native LVOT, which is referred to as the neo-LVOT (35). Acquired LVOTO (narrow/blocked neo-LVOT) is associated with procedure-related death, conversion to surgery, or emergency percutaneous reintervention (22). MDCT-derived 3DCM can estimate the neo-LVOT using various valves with different implantation heights, guiding TMVR (35).

According to the latest Mitral Valve Academic Research Consortium criteria, LVOTO is classified as an increase in LVOT gradient of ≥10 mm Hg compared with baseline (36). In previous studies, which used MDCT for prediction of the minimal neo-LVOT area, 2 methods of neo-LVOT estimation were described. In 2 reports, manual planimetry was performed on cross-sectional images with a THV projected on the mitral annulus in the mid to late systolic phase, when the neo-LVOT area is smallest (22,35). Using this method, the suggested cut-off value for the neo-LVOT area with greatest discriminatory value for LVOTO was ≤170.0 mm^2 (22).

The other method uses an MDCT-derived 3D computational model of the left heart with a virtual THV implant that allows semiautomated calculation of the minimal neo-LVOT area through volumetric assessment. With the neo-LVOT identified, its 3D relation to the implanted THV, LV, and original LVOT becomes clear. Repeated fitting using various virtual implants and manipulating device type, size, cardiac phase, implant depth, and co-axiality within the mitral annular plane is possible (**Figure 5**). Because volumetric data concerning the LV and THV can be derived from the computational model, obstruction can be expressed as a fraction of the original LVOT. Other predictors for LVOTO in TMVR, such as the angle between the native LVOT and aorta, AML length, and septal wall thickness, may be evaluated in these models, allowing review of complex 3D structures in different hypothetical situations (22,37). Furthermore, strategies can be planned to tackle projected obstruction (e.g., simultaneous LVOT balloon inflation, LVOT post-dilatation, or alcohol septal ablation). As such, the model serves as a patient-specific, virtual training ground allowing serial testing prior to the planned high-risk procedure without clinical consequences. A study using this method found a cut-off value for the MDCT-derived neo-LVOT area of ≤189.4 mm^2 to have the greatest discriminatory value for post-TMVR LVOTO (9).

Direct comparisons of the clinical accuracy of neo-LVOT prediction in pre- and post-TMVR MDCT datasets using 3D computational models have demonstrated excellent correlation with high reproducibility and accuracy (9). Comparing predicted and post-TMVR neo-LVOT by manual planimetry of MDCT images has also shown reproducibility with low intraobserver and interobserver variability (22). Of note, performance of neo-LVOT prediction with MDCT planimetry and semiautomated MDCT-derived 3DCM have yet to be compared.

MULTIPHASE PLANNING IN LVOT ASSESSMENT. As experience with LVOTO in TMVR expands, it becomes evident that pre-procedural planning based on

FIGURE 5 Virtually Implanted Prosthetic Heart Valves With Calculated Neo-LVOT

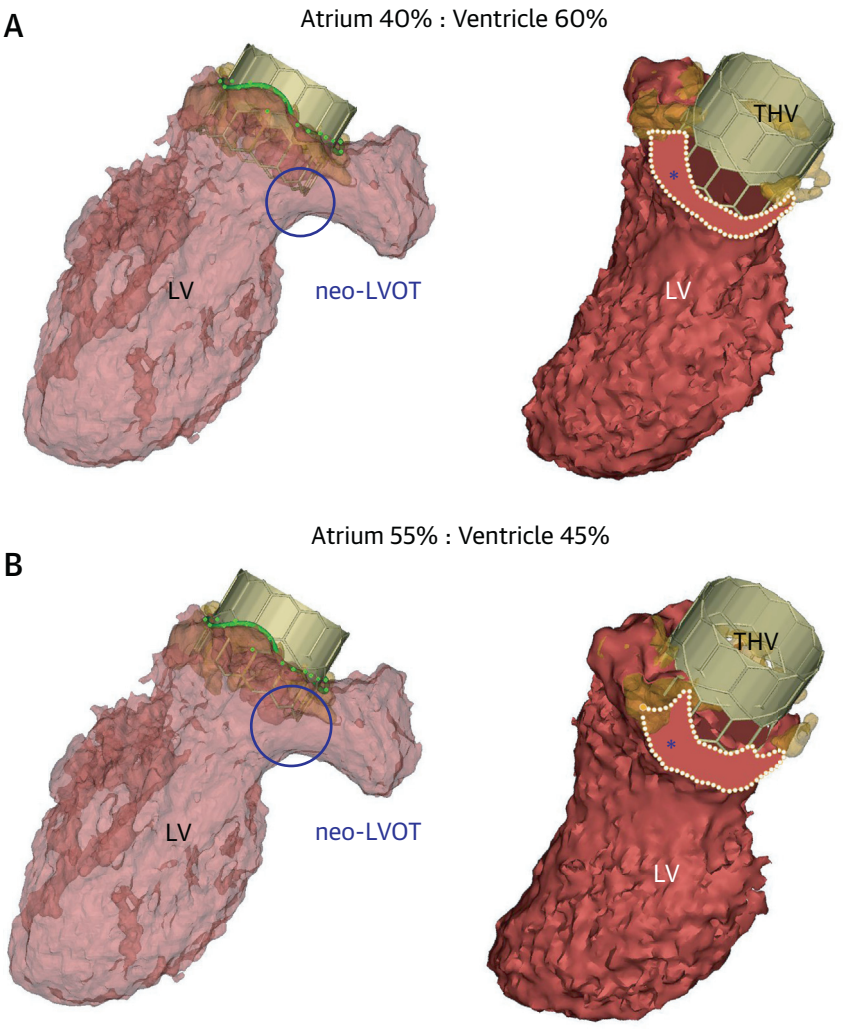

(A, right) MDCT-derived 3D computational model of the left ventricle (LV) with severely calcified mitral annulus **(yellow)** in a medio-lateral view. **(Left)** The same model viewed from the aorta. A virtual cylinder representing a 23-mm Sapien3 transcatheter heart valve (THV) was implanted at a 40/60 position. The neo left ventricular outflow tract (neo-LVOT) **(blue circle, left; blue asterisk, right)** is automatically calculated and has an area of 138 mm^2 (58% native LVOT occupancy). **(B)** The same LV model as in **A** with THV implanted at a 55/45 position. The calculated neo-LVOT area is 162 mm^2 (39% native LVOT occupancy). Abbreviations as in Figure 1.

a single cardiac phase might be too crude. As LVOT dimensions are smallest in the end-systole, around 40% of the R-R interval, any geometric LVOTO after TMVR would first occur in that phase. However, the vast majority of the stroke volume is ejected in the early and mid-systolic phase, implying that a functional, clinically relevant LVOTO should occur at that time. A report on pre-procedural multiphase neo-LVOT assessment in screening for TMVR using a dedicated THV showed that patients with predicted end-systolic obstruction performed well after TMVR when there was no predicted early systolic obstruction (38). These findings underpin the relevance of a multiphase approach when evaluating TMVR eligibility. The creation of full-cycle MDCT-derived 3D computational models, or 4D computational models, will add to effective patient/device selection in TMVR.

EVALUATING THE TRANSSEPTAL APPROACH. Transvenous transseptal TMVR is less invasive than the transapical approach and rapidly becoming the access strategy of first choice (25). Superior and

posterior puncture through the interatrial septum facilitates catheter manipulation in the LA for device orientation and positioning within the mitral apparatus. MDCT can provide a roadmap and help determine optimal C-arm angles that may be fused with live fluoroscopic imaging (39). MDCT-derived 3D computational models enhance appreciation of the anatomic relations among the inferior vena cava, interatrial septum, and mitral annulus. Additionally, by printing a 3D model of the right atrium, LA, and mitral annulus, the operator can undertake hands-on assessment of the transseptal puncture site. The optimal puncture site can be pre-determined followed by evaluation of the consequences for catheter manipulation when approaching the mitral valve. Furthermore, catheters can be tested in terms of flexibility, crossability, and deliverability toward the region of interest.

OPTIMAL FLUOROSCOPIC PROJECTIONS. Efforts have been made to determine MDCT-derived optimal fluoroscopic projections for TMVR (40). However, adequate visualization of the mitral annulus sometimes requires impractical angles in the catheter laboratory setting. Furthermore, optimal projections are device-specific and vary greatly between subjects. MDCT-derived 3DCM helps to compromise and determine the best workable fluoroscopic views for the respective TMVR-related manipulations (Supplemental Figure 1). Determining optimal projections prior to procedure commencement potentially reduces fluoroscopy time and therefore radiation exposure as well as contrast dosage (41).

PLANNING WITH DEDICATED DEVICES. Numerous dedicated devices that have proprietary anchoring mechanisms with unique spatial orientations in the LA, LV, and LVOT are being developed for TMVR (25). Planning TMVR with MDCT-derived 3D computational models may add substantially to determining the appropriate device for an individual patient.

For example, the Tendyne device (Abbott, Abbott Park, Illinois) utilizes an apical tethering mechanism for device stabilization (28) (Supplemental Figure 2). The anchoring zone of the tether is in a coaxial position with the LV apex. Deviations from that position could lead to loss of or excessive traction on the valve, resulting in suboptimal placement or dislocation of the valve. Identifying the optimal anchoring zone relies on 3D MDCT imaging with subsequent confirmation by procedural TEE and manual examination (42). In MDCT, the mitral annulus is manually traced using both short- and long-axis views leading to the formation of a virtual segmented annulus.

From this 3D annulus, a best-fit annular plane is computed using the least-squares method. This plane can be used to derive the geometric centroid of the mitral annulus (Supplemental Figure 2A). The ideal anchoring point is obtained by drawing a line perpendicular to the annular plane down to the epicardium of the LV. The suggested anchoring point for the tether is referred to as the orthogonal LV access point (Supplemental Figures 2B to 2D) (43). Once the anchoring site is determined, the device can be virtually implanted and assessed for adequate fit and relation to the LVOT. 3D modeling provides an overview of complex interlinked structures that determine suitability for a dedicated THV.

CLINICAL APPLICATIONS OF 3D COMPUTATIONAL MODELING: MITRAL PARAVALVULAR LEAKAGE CLOSURE

Significant prosthetic PVL after surgical mitral valve replacement is relatively common and reported in up to 17% of patients at 15 years of follow-up (44). Risk factors include annular calcification, infection, suture technique, tissue integrity, and myocardial contraction (45).

Echocardiography is the first step to reveal PVL location and quantification (46). Accurate orifice sizing is difficult as a result of dropout artifacts and may lead to underestimation of severity. Preprocedural MDCT assessment helps define PVL characteristics, strategy planning, and device/size selection. All MDCT imaging is associated with blooming and device-related artifacts that may impede accurate evaluation of valve integrity or leak sizing (12,47). However, when MDCT data is segmented to create a 3D model, it has the potential to partially bypass excessive artifacts (at the cost of variability). MDCT-derived 3DCM and virtual transcatheter closure device may improve accuracy and offer complementary insights into interstructural relations and sizing.

Determination of the cardiac phase is essential for PVL analysis and is in systole for mitral PVL. Finding the optimal phase is refined by additional TEE information (48). To obtain a 3D computational model from MDCT images, manual segmentation of the cardiac walls is required based on subtle differences in pixel gray value of the raw dataset. This is performed in the double oblique setting. From this segmentation, a 3D computational model is created. After manual adjustment, a patient-tailored model is created in which prosthesis shadowing and blooming artifacts are reduced to reveal essential details for

FIGURE 6 Pre-Procedural Assessment of Mitral Prosthetic Paravalvular Leak

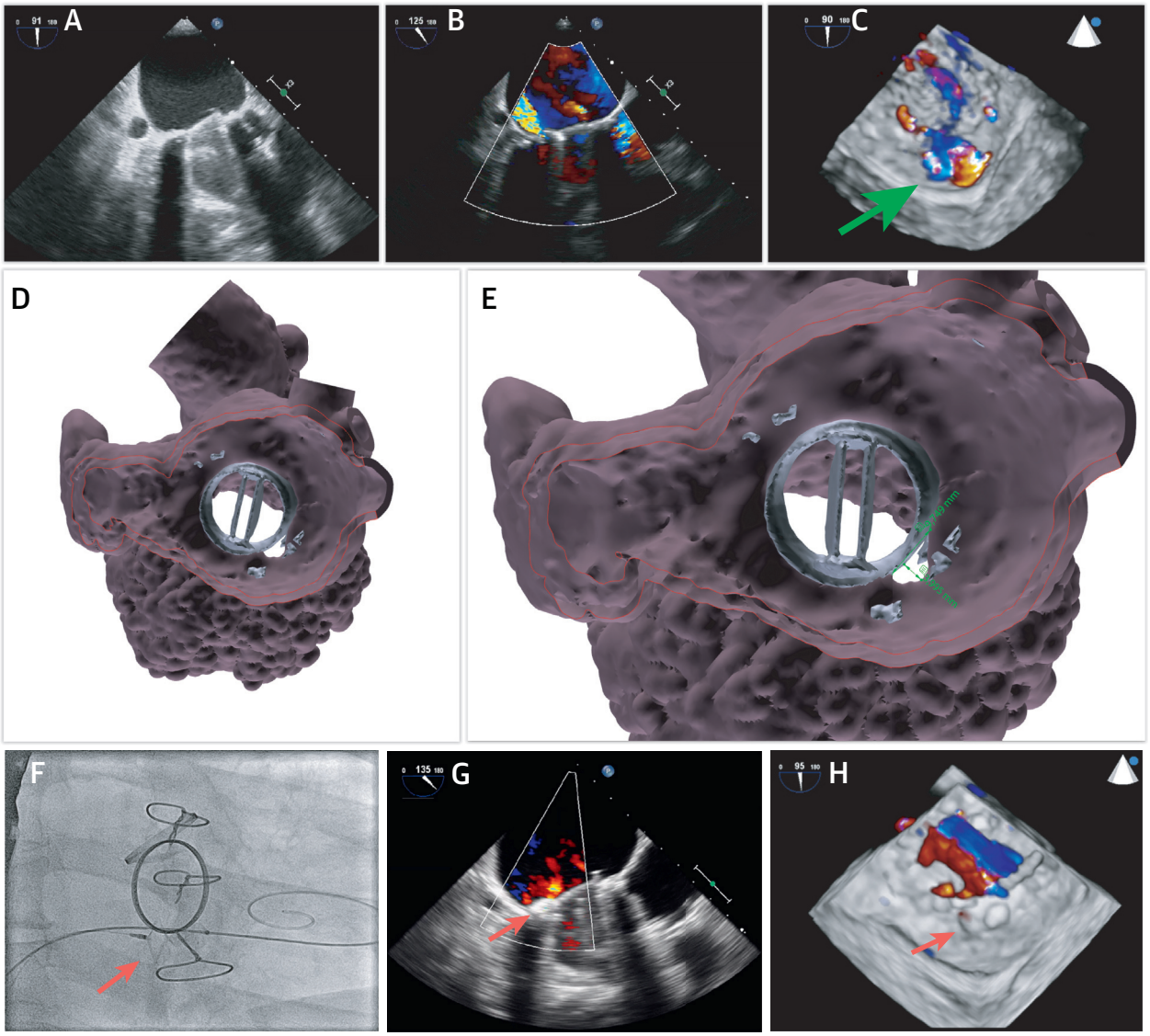

Images are obtained from a patient with a St. Jude 27-mm mechanical mitral prosthesis. **(A)** Transesophageal echocardiography (TEE) image in the 2-chamber view showing the mitral valve with no obvious paravalvular defect. **(B)** The same 2-chamber image with color-Doppler demonstrating a significant paravalvular leakage (PVL) on the postero-medial side of the prosthesis. **(C)** 3D-TEE image with color Doppler showing a PVL **(green arrow)**. **(D)** Pre-procedural, MDCT-derived 3D computational model of the prosthetic mitral valve from a surgical view in early diastole, the paravalvular defect is apparent on the postero-medial side. **(E)** Surgical view of the 3D reconstructed mitral prosthesis—the paravalvular defect measures 9.7 × 4.0 mm. **(F)** Based on measurements derived from the model in **D and E**, a 10 × 5 mm Amplatzer cardiac plug (Abbott, Abbott Park, Illinois) **(red arrow)** was selected. **(G)** Post-implantation TEE with the plug in situ **(red arrow)** showing reduced PVL. **(H)** 3D-TEE with color Doppler of the occluded PVL with the plug visible **(red arrow)**. Abbreviations as in Figure 1.

complex lesion sizing. Additionally, MDCT-derived 3DCM provides information on PVL location in relation to the inter-atrial septum and determination of an optimal catheter trajectory. Indeed, such modeling can determine whether percutaneous PVL closure is feasible at all (49). However, detailed knowledge about normal appearances as well as suture appearances is essential. To further clarify anatomic relations, the virtual model can be printed allowing bench testing (Figure 4B).

Figures 6A to 6C provide TEE illustration of PVL affecting a mechanical prosthetic mitral valve. Because the dimensions of the leak could not be adequately appreciated on these images, a

CENTRAL ILLUSTRATION **Pre-Procedural Planning of Mitral Valve Interventions Using MDCT-Derived 3-Dimensional Virtual and Printed Models**

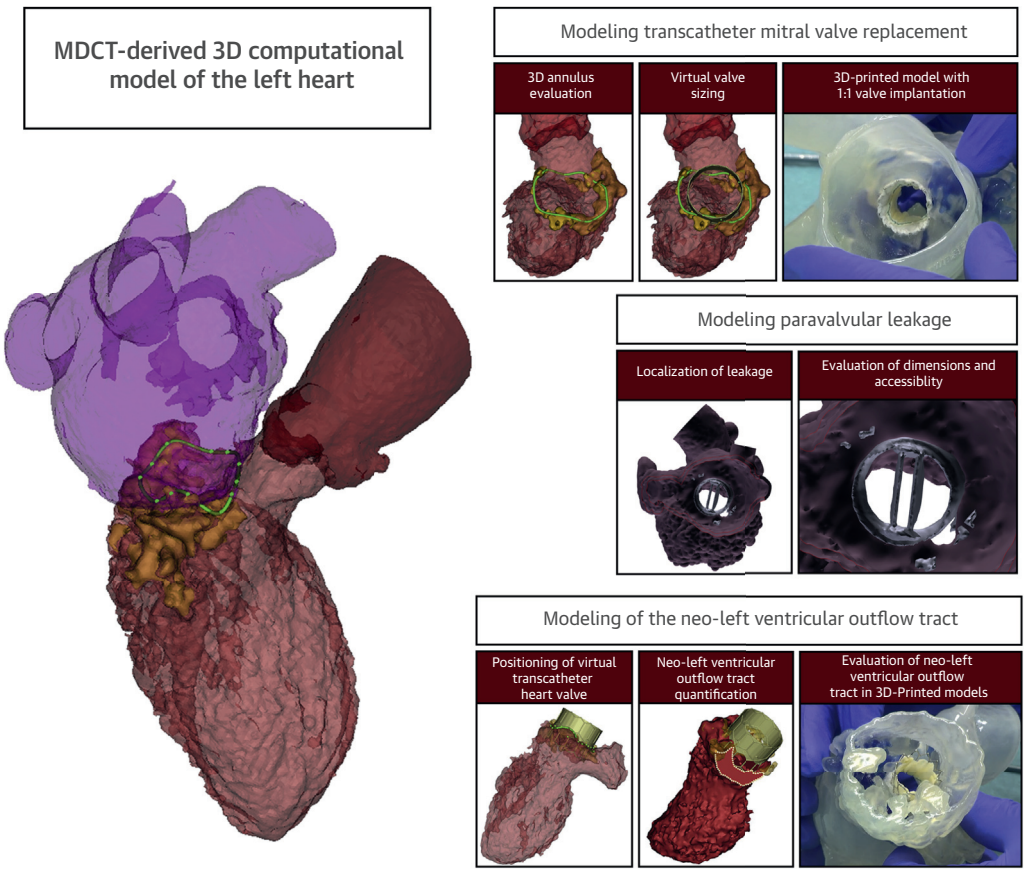

Ooms, J.F. et al. J Am Coll Cardiol Img. 2021;■(■):■–■.

MDCT-derived, 3-dimensional (3D), computational modeling and physical printing generate anatomic insights to help test, plan, and execute transcatheter mitral valve replacement and paravalvular leakage closure. MDCT = multidetector computed tomography.

complementary MDCT-derived 3D computational model was obtained, allowing measurements from different angles to enable appropriate sizing and closure device selection. Procedural results are depicted in Figures 6D to 6H.

In our experience, compared with TEE, MDCT-derived 3DCM provides superior information concerning location, sizing, and structural interactions of the lesion at hand when planning transcatheter PVL closure.

LIMITATIONS OF MDCT-DERIVED PRE-PROCEDURAL MODELING

MDCT ACQUISITION. MDCT has its inherent limitations. Its acquisition can be limited by arrhythmias or low cardiac output resulting in reduced luminal contrast. Additionally, it exposes patients to nephrotoxic contrast and could evoke allergic contrast reactions. In patients with renal dysfunction, prophylactic fluid administration prior to scan acquisition might induce variability in loading conditions. MDCT-derived modeling requires image acquisition throughout the entire cardiac cycle, and thus comes with additional ionizing radiation dose exposure.

MDCT-DERIVED 3D COMPUTATIONAL AND PRINTED MODELS. An MDCT-derived 3D computational model represents a static model and therefore only approximates real-time cardiac dynamics. Each segmented model is derived from 1 cardiac phase, which stresses the importance of adequate phase selection (i.e., expected dimensions being minimal/maximal). Currently, MDCT-derived 3D models do not allow for

shifting between phases once segmentation has been performed. Consequently, acquiring a model of the whole cardiac cycle requires laborious separate model segmentation and construction of each phase. Automation in segmentation could solve these issues. 3Dp relies on a single cardiac phase, making it less suitable for the evaluation of dynamic obstruction. Furthermore, important hemodynamic concepts and procedural hemodynamic filling status are not considered in a static model and may result in inaccurate sizing in vivo. The lack of incorporation of specific device and tissue properties in current MDCT-derived geometric models poses a problem when devices are implanted in real life. Although virtual device implantation may suggest a proper fit, in vivo implantation may cause marked tissue shift or altered device configuration leading to malapposition or rotation. Moreover, the absence of standardized protocols for device sizing in virtual 3D models could lead to interobserver variability. 3D-printed models are increasingly acquired to assist in pre-procedural planning of transcatheter structural heart interventions. However, cautious interpretation of their significance is necessary because these models still are a relatively raw representation of reality. Additionally, they lack standardized, reproducible methods for measuring distances/areas. However, efforts for structured verification have been made (50).

FUTURE DIRECTIONS

Several developments could further enhance MDCT-derived 3D modeling and will contribute to a future of patient-tailored valve replacement.

INCORPORATION OF TISSUE AND DEVICE PROPERTIES IN COMPUTATIONAL MODELING. In vivo implanted devices will affect the geometry/configuration of surrounding tissue and vice versa (51). Incorporation of tissue/device mechanical properties and their geometry and dimensions in a computational model predicts these geometric/configurational changes and, thereby, assists in the selection of the optimal device type and size (7,52). Patient-specific geometry is obtained from actual patient data (MDCT, CMR, 3D echo) and used to create a static model. Mechanical properties are derived from ex vivo stress-strain analyses. These experiments assess the changes in configuration/dimension of a structure upon exposure of stress. The changes in configuration depend on the amount and direction of the stress, the composition, and the reference state of the material (7,53). Computer modeling and simulation use finite element analysis to allow modeling of the whole (complex) structure (20,54,55). In TMVR, several cases are described in which a finite element model was used to predict outcome and aid pre-procedural planning. By incorporation of mechanical properties of the annulus, its calcium, the leaflets, and the selected THV, a simulation could be run predicting valve-fit and potential LVOTO (15,55,56). The current experience is proof of concept. Larger-scale validation studies are needed.

COMPUTATIONAL FLOW DYNAMICS AND FLUID-STRUCTURE INTERACTION MODELING. Incorporation of computational fluid dynamics (CFD) into MDCT-derived 3D computational models allows the assessment and quantification of PVL. These models can also be used to evaluate the effect of valve size, type, and depth of implantation on hemodynamics and therefore, the degree of functional LVOTO. It should be acknowledged that the CFD models are based on a number of assumptions such as pressure gradients, viscosity, and flow characteristics. Laminar and/or turbulent flow patterns are incorporated (55).

In addition to the above, analysis of the Fluid Structure Interaction (FSI) can conceptually be used for the assessment of the effects of the interaction between a fluid and adjacent structures (i.e., blood vs. valve/cardiac tissue). Resulting in the analysis of the changes in flow and flow patterns, pressures, and the subsequent effects on cardiac structures (53,57). For instance, it might facilitate prediction of the effect of dimensional changes in LVOT after TMVR, inducing a systolic anterior motion of the AML through pressure differences (Venturi effect) that in turn affect neo LVOT flow. In addition of the prediction of hemodynamics, FSI may be of particular value of the assessment of valve durability as (unwanted) flow patterns may induce endothelial cell changes (58). Although progress has been made in creating FSI models of individual components associated with mitral valve replacement (53,57), full TMVR models are experimental, are scarce, and cover only part of the interactions (55).

A TMVR model fully incorporating tissue and device properties; flow dynamics; fluid-structure interaction models; and coupling of LV, LA, and aorta may further improve hemodynamic prediction after structural heart interventions and will lead to an ultimate form of patient-tailored medicine, in which a valve is selected (or created) based on individual simulations (54,59). However, given the complex nature of these models and the computational power

required to create them, there is still a long road ahead for clinical adoption.

BIOPRINTING. Most 3Dp materials aim to mimic cardiac tissues. However, using actual (vivo) cardiovascular tissue might provide a solution for the crude biomechanical representation of the human heart in 3Dp. 3Dp using vivo tissue is referred to as bioprinting and the material used for printing is called bioink. This material comprises a viscoelastic medium (mostly hydrogels) together with cells. Depending on the cardiac structure required, bioink is often printed on a scaffold (3D geometric structure), which can be either biological or synthetic and could be modelled according to a patient's anatomy (60). Although the recreation of a fully functioning, patient-specific, biological 3D print of the heart is somewhat futuristic at this point, progress has been made on separate parts (61,62). Future incorporation of tissue into the patient-specific anatomy could greatly enhance the performance and authenticity of physical 3D-printed models in valvular heart disease leading to increased reliability in pre-procedural bench testing.

VIRTUAL REALITY AND HOLOGRAPHIC PROJECTION. 3D virtual models are presented on a 2D screen. Moreover, while 3Dp introduces a true 3D representation, it is time-consuming, expensive, and limited by the intrinsic characteristics of the material used (4). Visualizing virtual 3D models as holograms could bypass the need for physical printing, while still assessing the model in 3D space as if it were directly in front of the viewer (Supplemental Figure 3). Measurements can be made and the optimal strategy determined (63) while a connection to surgical tools or catheter wires may allow live integration of the intended procedure (64).

LIVE FUSION OF IMAGES. Integration or live-fusion of the MDCT-derived model with fluoroscopy may further optimize complex structural heart interventions. Fusion of the pre-procedural, 3D MDCT model and real-time procedural fluoroscopy may accelerate procedure execution, limit radiation, and increase safety (i.e., femoral and transseptal puncture, embolic protection placement, and valve deployment) (65).

HIGHLIGHTS

- Catheter-based interventions for complex defects of the mitral valve apparatus are evolving.
- MDCT-derived 3D computational modeling and 3D printing enhance risk evaluation and planning of complex transcatheter procedures.
- Incorporation of multiple cardiac phases, tissue/device properties, and hemodynamics should optimize 3D modeling.

CONCLUSIONS

MDCT-derived 3DCM, and physical printing generate unprecedented anatomic insights to help test, plan, and execute complex transcatheter mitral valve interventions (**Central Illustration**). Further research is needed to establish these advanced techniques in clinical practice.

FUNDING SUPPORT AND AUTHOR DISCLOSURES

Dr. Wang has served as a consultant for Edwards Lifesciences, Boston Scientific, and Materialise. Dr. Redwood has served as a proctor and consultant for Edwards Lifesciences. Dr. Popma has received institutional grants from Medtronic, Boston Scientific, Edwards Lifesciences, and Abbott; and is a member of the Medical Advisory Board of Edwards Lifesciences. Dr. Little has served as a consultant for Abbot Cardiovascular and Medtronic; and has received a research grant from Siemens Health. Dr. Pfeiffer has served as a consultant for LivaNova Inc.; and has served as a speaker and proctor for Edwards Lifesciences and Abbott Cardiovascular. Dr. Dahle has served as a proctor for Abbot Cardiovascular. Mrs. Minet is a former employee of Materialise NV. Dr. O'Neill has served as a consultant for Boston Scientific. Dr. Van Mieghem has received research grant support from Abbott, Boston Scientific, Edwards Lifesciences, and Medtronic; and has served as a consultant for Abbott, Boston Scientific, Edwards Lifesciences, Medtronic, Pie Medical, and Materialise NV. All other authors have reported that they have no relationships relevant to the contents of this paper to disclose.

ADDRESS OF CORRESPONDENCE: Dr. Nicolas M. Van Mieghem, Department of Interventional Cardiology, Thoraxcenter, Erasmus Medical Center, Room Nt-645, Dr. Molewaterplein 40, 3015 GD Rotterdam, the Netherlands. E-mail: n.vanmieghem@erasmusmc.nl.

REFERENCES

1. Binder RK, Webb JG, Willson AB, et al. The impact of integration of a multidetector computed tomography annulus area sizing algorithm on outcomes of transcatheter aortic valve replacement: a prospective, multicenter, controlled trial. J Am Coll Cardiol 2013;62:431–8.

2. Faletra FF, Pedrazzini G, Pasotti E, et al. 3D TEE during catheter-based interventions. J Am Coll Cardiol Img 2014;7:292–308.

3. El Sabbagh A, Eleid MF, Matsumoto JM, et al. Three-dimensional prototyping for procedural simulation of transcatheter mitral valve replacement in patients with mitral annular calcification. Catheter Cardiovasc Interv 2018;92:E537–49.

4. Tuncay V, van Ooijen PMA. 3D printing for heart valve disease: a systematic review. Eur Radiol Exp 2019;3:9.

5. Kohli K, Wei ZA, Yoganathan AP, Oshinski JN, Leipsic J, Blanke P. Transcatheter mitral valve planning and the neo-LVOT: utilization of virtual simulation models and 3D printing. Curr Treat Options Cardiovasc Med 2018;20:99.

6. Ripley B, Kelil T, Cheezum MK, et al. 3D printing based on cardiac CT assists anatomic visualization prior to transcatheter aortic valve replacement. J Cardiovasc Comput Tomogr 2016;10:28–36.

7. de Jaegere P, Rocatello G, Prendergast BD, de Backer O, Van Mieghem NM, Rajani R. Patient-specific computer simulation for transcatheter cardiac interventions: what a clinician needs to know. Heart 2019;105:s21–7.

8. Byrne N, Velasco Forte M, Tandon A, Valverde I, Hussain T. A systematic review of image segmentation methodology, used in the additive manufacture of patient-specific 3D printed models of the cardiovascular system. JRSM Cardiovasc Dis 2016;5:2048004016645467.

9. Wang DD, Eng MH, Greenbaum AB, et al. Validating a prediction modeling tool for left ventricular outflow tract (LVOT) obstruction after transcatheter mitral valve replacement (TMVR). Catheter Cardiovasc Interv 2018;92:379–87.

10. Wang DD, Eng M, Greenbaum A, et al. Predicting LVOT obstruction after TMVR. J Am Coll Cardiol Img 2016;9:1349–52.

11. Vukicevic M, Mosadegh B, Min JK, Little SH. Cardiac 3D printing and its future directions. J Am Coll Cardiol Img 2017;10:171–84.

12. Newland JA, Tamuno P, Pasupati S, et al. Emerging role of MDCT in planning complex structural transcatheter intervention. J Am Coll Cardiol Img 2014;7:627–31.

13. Hermsen JL, Burke TM, Seslar SP, et al. Scan, plan, print, practice, perform: Development and use of a patient-specific 3-dimensional printed model in adult cardiac surgery. J Thorac Cardiovasc Surg 2017;153:132–40.

14. Legget ME, Bashein G, McDonald JA, et al. Three-dimensional measurement of the mitral annulus by multiplane transesophageal echocardiography: in vitro validation and in vivo demonstration. J Am Soc Echocardiogr 1998;11:188–200.

15. Karady J, Ntalas I, Prendergast B, et al. Transcatheter mitral valve replacement in mitral annulus calcification - "The art of computer simulation." J Cardiovasc Comput Tomogr 2018;12:153–7.

16. Batteux C, Haidar MA, Bonnet D. 3D-printed models for surgical planning in complex congenital heart diseases: a systematic review. Front Pediatr 2019;7:23.

17. Vukicevic M, Puperi DS, Jane Grande-Allen K, Little SH. 3D printed modeling of the mitral valve for catheter-based structural interventions. Ann Biomed Eng 2017;45:508–19.

18. Farooqi KM, Cooper C, Chelliah A, et al. 3D printing and heart failure: the present and the future. J Am Coll Cardiol HF 2019;7:132–42.

19. Fan Y, Wong RHL, Lee AP. Three-dimensional printing in structural heart disease and intervention. Ann Transl Med 2019;7:579.

20. Rausch MK, Famaey N, Shultz TO, Bothe W, Miller DC, Kuhl E. Mechanics of the mitral valve: a critical review, an in vivo parameter identification, and the effect of prestrain. Biomech Model Mechanobiol 2013;12:1053–71.

21. Iung B, Delgado V, Rosenhek R, et al. Contemporary Presentation and management of valvular heart disease: the EURObservational Research Programme Valvular Heart Disease II Survey. Circulation 2019;140:1156–69.

22. Yoon SH, Bleiziffer S, Latib A, et al. Predictors of left ventricular outflow tract obstruction after transcatheter mitral valve replacement. J Am Coll Cardiol Intv 2019;12:182–93.

23. Van Mieghem NM, Piazza N, Anderson RH, et al. Anatomy of the mitral valvular complex and its implications for transcatheter interventions for mitral regurgitation. J Am Coll Cardiol 2010;56:617–26.

24. Yoon SH, Whisenant BK, Bleiziffer S, et al. Outcomes of transcatheter mitral valve replacement for degenerated bioprostheses, failed annuloplasty rings, and mitral annular calcification. Eur Heart J 2019;40:441–51.

25. Regueiro A, Granada JF, Dagenais F, Rodes-Cabau J. Transcatheter mitral valve replacement: insights from early clinical experience and future challenges. J Am Coll Cardiol 2017;69:2175–92.

26. Guerrero M, Dvir D, Himbert D, et al. Transcatheter mitral valve replacement in native mitral valve disease with severe mitral annular calcification: results from the first multicenter global registry. J Am Coll Cardiol Intv 2016;9:1361–71.

27. Guerrero M, Urena M, Himbert D, et al. 1-year outcomes of transcatheter mitral valve replacement in patients with severe mitral annular calcification. J Am Coll Cardiol 2018;71:1841–53.

28. Moat N, Duncan A, Lindsay A, et al. Transcatheter mitral valve replacement for the treatment of mitral regurgitation: in-hospital outcomes of an apically tethered device. J Am Coll Cardiol 2015;65:2352–3.

29. Sucha D, Daans CG, Symersky P, et al. Reliability, agreement, and presentation of a reference standard for assessing implanted heart valve sizes by multidetector-row computed tomography. Am J Cardiol 2015;116:112–20.

30. Rajani R, Attia R, Condemi F, et al. Multidetector computed tomography sizing of bioprosthetic valves: guidelines for measurement and implications for valve-in-valve therapies. Clin Radiol 2016;71:e41–8.

31. Blanke P, Dvir D, Cheung A, et al. Mitral annular evaluation with CT in the context of transcatheter mitral valve replacement. J Am Coll Cardiol Img 2015;8:612–5.

32. Leipsic J, Blanke P. Calcification of the aortic valve and mitral apparatus: location, quantification and implications for device selection. EuroIntervention 2016;12:Y16–20.

33. Abramowitz Y, Jilaihawi H, Chakravarty T, Mack MJ, Makkar RR. Mitral annulus calcification. J Am Coll Cardiol 2015;66:1934–41.

34. Come PC, Riley MF, Weintraub RM, et al. Dynamic left ventricular outflow tract obstruction when the anterior leaflet is retained at prosthetic mitral valve replacement. Ann Thorac Surg 1987;43:561–3.

35. Blanke P, Naoum C, Dvir D, et al. Predicting LVOT obstruction in transcatheter mitral valve implantation: concept of the neo-LVOT. J Am Coll Cardiol Img 2017;10:482–5.

36. Stone GW, Adams DH, Abraham WT, et al. Clinical trial design principles and endpoint definitions for transcatheter mitral valve repair and replacement: part 2: endpoint definitions: a consensus document from the Mitral Valve Academic Research Consortium. Eur Heart J 2015;36:1878–91.

37. Bapat V, Pirone F, Kapetanakis S, Rajani R, Niederer S. Factors influencing left ventricular outflow tract obstruction following a mitral valve-in-valve or valve-in-ring procedure, part 1. Catheter Cardiovasc Interv 2015;86:747–60.

38. Meduri CU, Reardon MJ, Lim DS, et al. Novel multiphase assessment for predicting left ventricular outflow tract obstruction before transcatheter mitral valve replacement. J Am Coll Cardiol Intv 2019;12:2402–12.

39. Van Mieghem NM, Rodriguez-Olivares R, Ren BC, et al. Computed tomography optimised fluoroscopy guidance for transcatheter mitral therapies. EuroIntervention 2016;11:1428–31.

40. Blanke P, Dvir D, Naoum C, et al. Prediction of fluoroscopic angulation and coronary sinus location by CT in the context of transcatheter mitral valve implantation. J Cardiovasc Comput Tomogr 2015;9:183–92.

41. Hell MM, Biburger L, Marwan M, et al. Prediction of fluoroscopic angulations for transcatheter aortic valve implantation by CT angiography: influence on procedural parameters. Eur Heart J Cardiovasc Imaging 2017;18:906–14.

42. Duncan A, Daqa A, Yeh J, et al. Transcatheter mitral valve replacement: long-term outcomes of first-in-man experience with an apically tethered device- a case series from a single centre. EuroIntervention 2017;13:e1047–57.

43. Blanke P, Park JK, Grayburn P, et al. Left ventricular access point determination for a coaxial approach to the mitral annular landing zone in transcatheter mitral valve replacement. J Cardiovasc Comput Tomogr 2017;11:281–7.

44. Hammermeister K, Sethi GK, Henderson WG, Grover FL, Oprian C, Rahimtoola SH. Outcomes 15 years after valve replacement with a mechanical versus a bioprosthetic valve: final report of the Veterans Affairs randomized trial. J Am Coll Cardiol 2000;36:1152–8.

45. Safi AM, Kwan T, Afflu E, Al Kamme A, Salciccioli L. Paravalvular regurgitation: a rare complication following valve replacement surgery. Angiology 2000;51:479–87.

46. Kinno M, Raissi SR, Olson KA, Rigolin VH. Three-dimensional echocardiography in the evaluation and management of paravalvular regurgitation. Echocardiography 2018;35:2056–70.

47. Koo HJ, Lee JY, Kim GH, et al. Paravalvular leakage in patients with prosthetic heart valves: cardiac computed tomography findings and clinical features. Eur Heart J Cardiovasc Imaging 2018;19:1419–27.

48. Lancellotti P, Pibarot P, Chambers J, et al. Recommendations for the imaging assessment of

prosthetic heart valves: a report from the European Association of Cardiovascular Imaging endorsed by the Chinese Society of Echocardiography, the Inter-American Society of Echocardiography, and the Brazilian Department of Cardiovascular Imaging. Eur Heart J Cardiovasc Imaging 2016;17:589–90.

49. Hascoet S, Smolka G, Bagate F, et al. Multimodality imaging guidance for percutaneous paravalvular leak closure: Insights from the multi-centre FFPP register. Arch Cardiovasc Dis 2018;111:421–31.

50. Odeh M, Levin D, Inziello J, et al. Methods for verification of 3D printed anatomic model accuracy using cardiac models as an example. 3D Print Med 2019;5:6.

51. Schultz CJ, Weustink A, Piazza N, et al. Geometry and degree of apposition of the CoreValve ReValving system with multislice computed tomography after implantation in patients with aortic stenosis. J Am Coll Cardiol 2009;54:911–8.

52. de Jaegere P, De Santis G, Rodriguez-Olivares R, et al. Patient-specific computer modeling to predict aortic regurgitation after transcatheter aortic valve replacement. J Am Coll Cardiol Intv 2016;9:508–12.

53. Votta E, Le TB, Stevanella M, et al. Toward patient-specific simulations of cardiac valves: state-of-the-art and future directions. J Biomech 2013;46:217–28.

54. Rausch MK, Zollner AM, Genet M, Baillargeon B, Bothe W, Kuhl E. A virtual sizing tool for mitral valve annuloplasty. Int J Numer Method Biomed Eng 2017;33.

55. Pasta S, Cannata S, Gentile G, Agnese V, Pilato M, Gandolfo C. Simulation of left ventricular outflow tract (LVOT) obstruction in transcatheter mitral valve-in-ring replacement. Med Eng Phys 2020;82:40–8.

56. de Jaegere P, Rajani R, Prendergast B, Van Mieghem NM. Patient-specific computer modeling for the planning of transcatheter mitral valve replacement. J Am Coll Cardiol 2018;72:956–8.

57. Marom G. Numerical methods for fluid-structure interaction models of aortic valves. Archives of Computational Methods in Engineering 2015;22:595–620.

58. Sacks M, Drach A, Lee CH, et al. On the simulation of mitral valve function in health, disease, and treatment. J Biomech Eng 2019 Apr 20 [E-pub ahead of print].

59. Gao H, Qi N, Feng L, et al. Modelling mitral valvular dynamics-current trend and future directions. Int J Numer Method Biomed Eng 2017;33.

60. Alonzo M, AnilKumar S, Roman B, Tasnim N, Joddar B. 3D Bioprinting of cardiac tissue and cardiac stem cell therapy. Transl Res 2019;211:64–83.

61. Jana S, Lerman A. Bioprinting a cardiac valve. Biotechnol Adv 2015;33:1503–21.

62. Lee A, Hudson AR, Shiwarski DJ, et al. 3D bioprinting of collagen to rebuild components of the human heart. Science 2019;365:482–7.

63. Butera G, Sturla F, Pluchinotta FR, Caimi A, Carminati M. Holographic augmented reality and 3D printing for advanced planning of sinus venosus ASD/partial anomalous pulmonary venous return percutaneous management. J Am Coll Cardiol Intv 2019;12:1389–91.

64. De Paolis LT, De Luca V. Augmented visualization with depth perception cues to improve the surgeon's performance in minimally invasive surgery. Med Biol Eng Comput 2019;57:995–1013.

65. Vernikouskaya I, Rottbauer W, Seeger J, Gonska B, Rasche V, Wohrle J. Patient-specific registration of 3D CT angiography (CTA) with x-ray fluoroscopy for image fusion during transcatheter aortic valve implantation (TAVI) increases performance of the procedure. Clin Res Cardiol 2018;107:507–16.

KEY WORDS 3D printing, computational modeling, mitral annular calcification, multidetector computed tomography, paravalvular leakage closure, transcatheter mitral valve replacement

APPENDIX For supplemental figures, please see the online version of this paper.